Role of voids in granular convection

Troy Shinbrot, D. V. Khakhar, J. J. McCarthy, and Julio M. Ottino
Department of Chemical Engineering, Northwestern University, Evanston, Illinois 60208
(Received 3 September 1996)

We study the dynamics of voids in granular convection. First, we associate the formation of voids with the onset of convection, and thereby develop predictions for convective onset as a function of system parameters. Second, we use a stochastic approach to examine the role of void penetration in fully developed granular convection. We find that the vertical flow field should depend on the hyperbolic cosine of the horizontal coordinate and on a mixed linear-exponential function of the vertical coordinate. We present both lattice-based and particle-dynamic numerical simulations to validate this analysis, and provide several testable predictions. [S1063-651X(97)07905-1]

PACS number(s): 46.10.+z, 05.40.+j, 83.10.Hh

INTRODUCTION

Granular flow has been the focus of intensive experimental study over the past several years [1]. These investigations are driven by two, largely opposing, motivations. On the one hand, the variety of behaviors [1,2] that externally excited granular systems are subject to is unparalleled in fluid problems. On the other hand, there exist exceedingly few general principles [3] for the understanding or analysis of these systems.

Historically, one of the very few principles of granular flow that *has* been well recognized is the need for voids [4]. Without voids, grains remain trapped in an interlocked state that obstructs particle transport. With recent advances in computer technology, research has increasingly focused on particle-dynamics investigations, and in this respect the importance of void dynamics has been lost [5].

In this paper, we examine two implications of the need for voids in granular flow. In the first section, we derive a criterion for the onset of granular convection by assuming that grains can begin to flow only once voids emerge that are at least as large as the constituent particles themselves. In the second section, we analyze well-established convection. There, we treat the penetration of voids by particles as a chaotic scattering problem; this permits us to develop a stochastic model leading to a difference equation that governs convective flow. We test our analytic results with three distinct types of numerical simulations: hard-particle, lattice-based (cellular-automata), and soft-particle.

I. CONVECTIVE ONSET

If voids are required for the flow of granular material, then it follows that the emergence of voids should coincide with the onset of convection. Convection is typically produced in experiments by sinusoidally shaking a container [1,6,7]. The complete problem of how voids are created in a container containing a large number of grains is difficult [8] and we do not attempt to solve it here. Instead, we observe that granular materials typically collide inelastically with container walls [9], so it is appropriate as a first approximation to solve the problem of a single inelastic mass resting on the bottom of a vibrating container [8,10]. In this case, we can establish conditions under which the mass will become airborne and we can compute the maximum distance $h_{\max}$ between the bottom of such a mass and the bottom of the container [see Fig. 1(a)]. We conjecture that when $h_{\max}$ exceeds the characteristic particle diameter d, it may be possible for particles to flow. While this criterion for the onset of convection is only approximate, it can be expressed analytically and, as will be shown, it shares similarities with existing experimental data.

Throughout this paper we neglect aerodynamic forces; the results are thus suitable for experiments executed in a vacuum or for other problems in which drag or trapped air can be neglected. There is extensive literature on the behavior of masses subjected to harmonic shaking [8,11], so we only briefly review the key points here. In Fig. 1(b), we plot as a solid line the vertical position of a harmonically vibrated platform. A mass supported by the platform will become airborne when the platform's downward acceleration exceeds gravity g, that is, when

$$g = A\omega^2 \sin(\omega t) \tag{1}$$

or

$$t = t_0 = \sin^{-1}\left(\frac{g}{A\omega^2}\right). \tag{2}$$

After leaving the platform, the vertical position of the bottom of the mass will obey

$$z = \left(\frac{g}{2}\right)(t-t_0)^2 + [A\omega\ \cos(\omega t_0)](t-t_0) + [A\ \sin(\omega t_0)]. \tag{3}$$

This parabolic trajectory terminates once the mass strikes the platform again. After this point, the mass may again become airborne. The resulting vertical position of the mass is depicted in Fig. 1(b) as shaded circles.

At some point, the height of the mass above the platform achieves a maximum, denoted $h_{\max}$ in Fig. 1(b). As we have indicated, our motivating conjecture is that the onset of convection occurs when $h_{\max}$ exceeds the particle diameter d, which, for simplicity, we take to be a constant. In Fig. 2, we plot the dependence of the frequency ω on the amplitude of

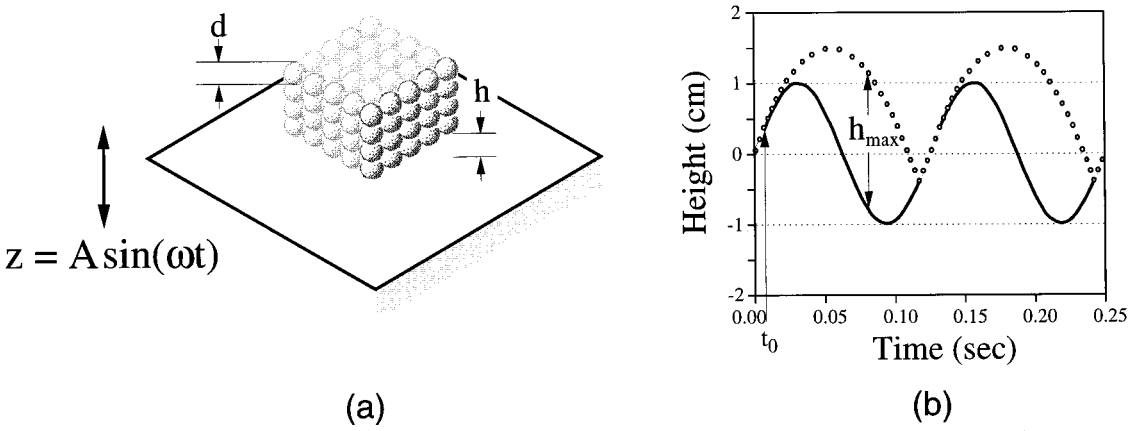

FIG. 1. (a) Inelastic mass of particles on a vibrating platform, with diameter of particles d and height of mass above platform h indicated. (b) Position of platform (solid line) and of mass (circles) for platform vibration given by $z=\sin(16\pi t)$.

shaking A, when this criterion for onset is met, for particle diameters ranging from 1 to 5 mm. For large amplitude oscillations, onset apparently occurs for frequencies that go as $\sqrt{A}$. This is what we would naively expect: since the platform's acceleration goes as $\Gamma\equiv A\omega^2$, constant acceleration lines lie along $\omega\sim 1/\sqrt{A}$. In the figure, we plot two lines, $\Gamma=g$ and $\Gamma=1.2g$. The first line is the minimal possible criterion for onset; below this acceleration, inelastic particles never become airborne. The second line corresponds to experimental reports of convective onset [12]. For vibration amplitudes on the order of 1 cm, our criterion for onset approximately coincides with experimental observations for all particle sizes [13] in the range 1–5 mm. Our results indicate that for lower amplitude vibrations, higher Γ values would be required to achieve onset. This effect should be especially pronounced for large particles. The converse is also true: higher amplitudes require slightly smaller values of Γ. Indeed, Fig. 2 indicates that slightly lower accelerations than have been reported to date may also induce convection, especially at large amplitude.

Also, for large amplitude oscillations we note that onset should occur at very nearly the same frequency, independent of particle size [13]. For small amplitude oscillations, by comparison, the frequency at onset should significantly increase with particle size. If we fix the amplitude, we can investigate this dependence by plotting $h_{\max}$ vs ω, as shown in the inset to Fig. 3. The asymptotic height $h_{\omega\to\infty}$ attained at large frequency is strictly proportional to the amplitude A, according to $h_{\omega\to\infty}=10.5A$. If we subtract the maximum height above the platform attained by the mass from this asymptotic height (i.e., compute $h_{\max}-h_{\omega\to\infty}$) and plot this difference as a function of frequency, we obtain the main plot of Fig. 3. From these results, we find that for sufficiently high frequency the following scaling relation is obeyed to a high degree of accuracy:

$$h_{\max}\cong 10.5A-\frac{48.3g}{\omega^2}. \tag{4}$$

By associating a particular grain diameter d with the height $h_{\max}$ as previously described, this equation provides an explicit prediction for the onset of convection. Moreover, in the following section we show that Eq. (4) can be used to predict the dependence of fully developed convection on driving parameters.

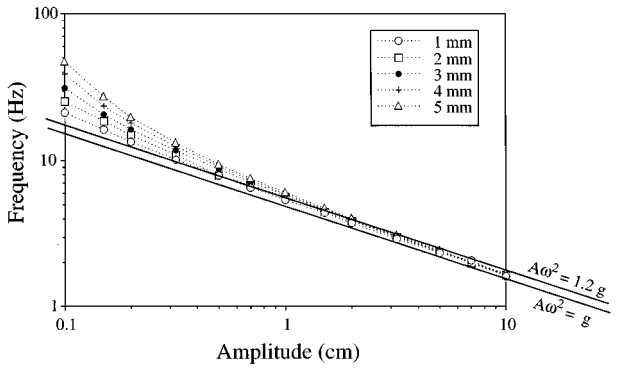

FIG. 2. Platform vibration frequency vs amplitude at theoretical convection onset for various size particles. Solid lines indicate the minimum possible onset criterion: a maximum acceleration $\Gamma=g$ and an often reported onset criterion $\Gamma=1.2g$.

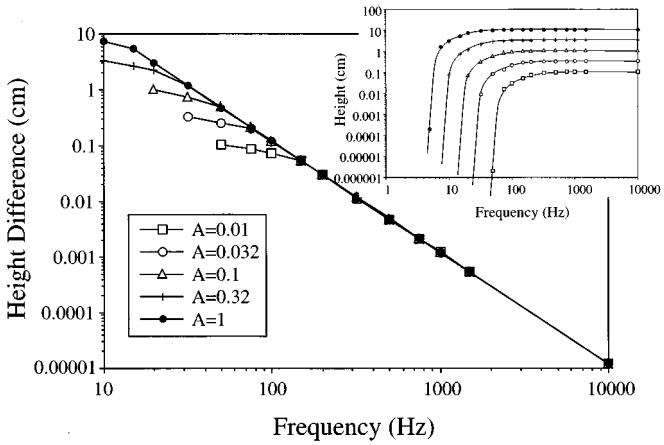

FIG. 3. Inset: height of mass above platform versus frequency of vibration for various amplitudes of vibration (defined in legend). Main plot: difference in height from high frequency asymptote versus frequency.

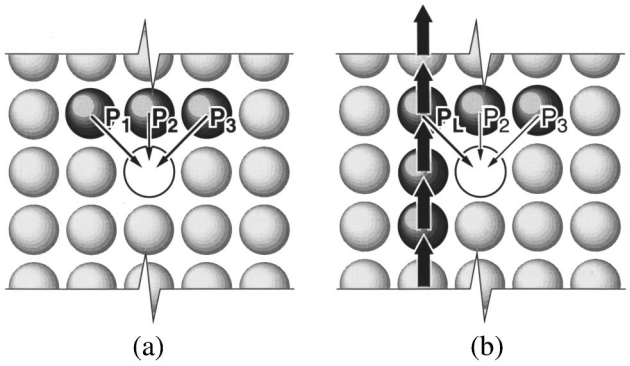

FIG. 4. (a) Probabilities for scattering of particles into void from above left (P_1), center (P_2), and right (P_3). (b) Scattering probabilities with relative velocity of one column. Here the probability that any particle might enter the void from the left is denoted P_L. Dark shaded particles can enter the void.

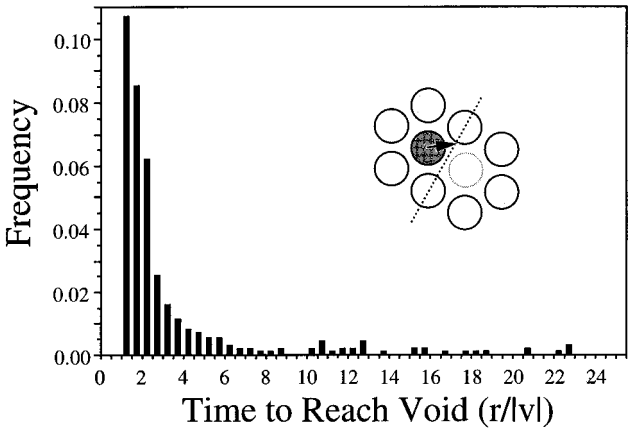

FIG. 5. Inset: hard-particle-dynamics scattering configuration, in which a single particle (dark gray) scatters with a random initial direction against initially stationary inelastic masses (light gray). Void penetration is judged according to whether or not the dark particle crosses the dotted line shown. Main plot: frequency of scattering into the void versus the time at which the penetration occurs (measured in units of particle separation per velocity maximum).

II. VOID PENETRATION AND CHAOTIC SCATTERING

A. Central conjecture

The idea here is as follows. Suppose we have a void in a two-dimensional (2D) granular material. We take the simplest case, where the grains are ordered in a rectangular [14] lattice, as shown in Fig. 4(a). Our analysis is not restricted to a lattice, but the use of a lattice considerably simplifies computational comparisons that follow (in particular, the identification of a void and the vertical velocity of a column of particles become quite clear-cut in a lattice). To determine how the flow will evolve, at a minimum we need to know which of the particles surrounding the void will ultimately fill it. The crucial observation is that this is a scattering problem among convex bodies, and it is known that this class of problem, even using stationary scatterers, is exquisitely sensitive to tiny variations in initial conditions [15]. This being the case, we turn to stochastic methods. All calculations that follow should be understood to apply to averages over very many realizations. We begin with the central conjecture that *the probability of penetrating a void should increase with the number of scattering opportunities* presented. This seemingly innocuous conjecture allows us to analytically solve a number of outstanding granular convection puzzles.

Consider first the situation depicted in Fig. 4(a): a lattice of particles with a single void. We analyze only the possibility of particles penetrating the void from above [16] and we assume that the void is typically filled in a characteristic time τ. Then the *a priori* probability that the void will be filled by a particle from the column to the left is

$$P_L=\frac{P_1}{P_1+P_2+P_3}. \tag{5}$$

By contrast, consider the situation shown in Fig. 4(b), where particles to the left of the void are taken to move vertically with fixed velocity V_L, measured in particle diameters per unit time. If m_L particles in the moving column pass by the void in time τ, then we expect the probability that the void will be filled by a particle from the left to increase correspondingly. Here, $m_L=1+V_L\tau$ and the probability to fill the void from the left is

$$P_L=\frac{m_L P_1}{m_L P_1+P_2+P_3}. \tag{6}$$

So, to take a numerical example, if $P_1=P_3=0.1P_2$ and $m_L=2$, then for the stationary case (5), $P_L=8\%$, while for the moving case (6), $P_L=15\%$. Thus the probability of penetrating a void can easily be doubled by increasing the relative velocity of particles passing by the void (in fact, $P_L\to 1$ as $m_L\to\infty$).

To prevent confusion, we remark that the relative velocity between the adjacent columns that we have referred to can be viewed in either of two ways, depending on context. In a problem where there is a characteristic time τ within which a void becomes filled, the relative vertical velocity ΔV is the quantity of interest and the number of opportunities presented to scatter into the void is just $\Delta V\tau$. In a problem where the system is agitated and returned to rest, the relative velocity can instead be viewed as the total *displacement* by which a column settles with respect to its neighbors in a unit settling time. We consider the latter case in this paper, however, to conform with existing nomenclature, we refer to this displacement as a velocity.

B. Tests of the conjecture

As we have said, this argument hinges on the assumption that a void is filled in a characteristic time τ. This is easily tested: in Fig. 5 we display results of a hard-particle-dynamic [17] simulation, in which a single particle (dark gray in inset) adjacent to a void is given an initial impulse of fixed amplitude $|v|$, but random direction. All other particles are initially stationary but are free to move. All particles are identical and have initial separation $s=1$ and radius $r=0.4s$. Collisions are inelastic with coefficient of restitution 0.75. The void is judged to have been penetrated once the dark

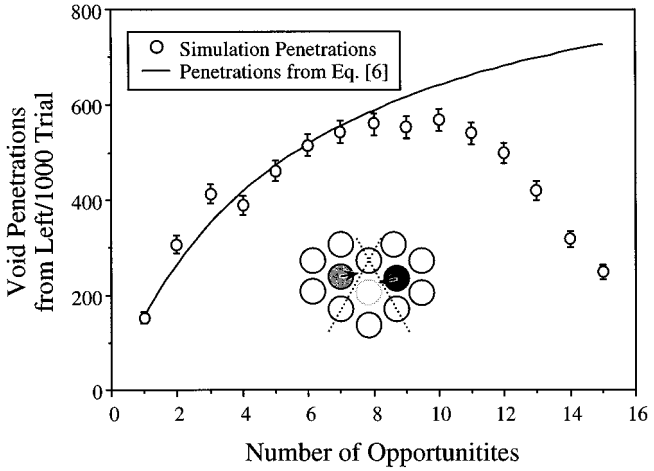

FIG. 6. Inset: hard-particle-dynamics scattering configuration for a void surrounded by a fixed lattice. Dark gray particle on left is provided multiple opportunities to penetrate the void; competing black particle on right has only one opportunity. Main plot: void penetration rate versus number of opportunities. Open circles give averages over 1000 trials; solid line is fit to Eq. (6).

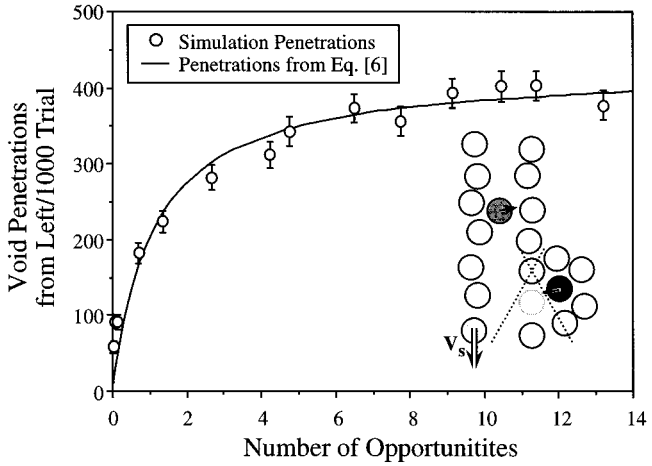

FIG. 7. Inset: hard-particle-dynamics scattering configuration for pseudocontinuum flow with imposed shear. Dark gray particle on left is provided multiple opportunities to penetrate the void by virtue of a wall to the left moving down with fixed velocity V_s. Competing black particle to the right of the void has only one opportunity. Main plot: void penetration rate versus number of opportunities. Open circles give averages over 1000 trials; solid line is fit to Eq. (6), modified to account for dark gray particle egress either through the bottom or through the void (see text).

particle crosses the dotted line shown in the inset to Fig. 5, separating the initial position of the dark particle from the void location. In the main part of the figure we plot a histogram of the frequency of penetration of the void by the dark particle versus the time taken to achieve the penetration. From this simulation of 1000 separate trials, we find that in excess of 92% of void penetrations occur within a fixed time, given by $\tau = 10r/|v|$. Thus, to a high degree of approximation, we can assume that voids are filled within this characteristic time. Similar simulations with immovable scatterers yield essentially identical results.

As a consequence of this calculation, we conclude that multiple scattering opportunities can enhance the overall scattering rate, provided that the time between opportunities is $\gg r/|v|$. We test this conclusion in two separate simulations, one bounded by particles fixed on a lattice and a second spatially continuous.

The first simulation, which we term ''pseudo-lattice-based,'' is shown in the inset to Fig. 6. Here we provide a particle on the left (dark gray) with M opportunities to scatter into a void in time $10r/|v|$. The particles surrounding the void (light gray) are immovable and are fixed on a hexagonal lattice. During the same time interval, a second particle (black) on the right of the void is given only a single opportunity. Technically, this is done by initially giving each particle a kick of fixed amplitude and random direction, and allowing the particles to compete to penetrate the void. Once every unit time $10r/(|v|M)$, the particle on the left is removed and a new particle is placed at the same initial location but with a new randomized kick direction. After a time $10r/|v|$, no further particle displacements occur, and the simulation is allowed to continue until both moving particles come to rest. Particle sizes, spacing, and coefficient of restitution are as before.

In the main plot of Fig. 6, we plot as open circles the resulting number of void penetrations from the left in 1000 trials as a function of the number of opportunities per trial, M. On the same plot, we include as a solid line the prediction from Eq. (6), using only the $M=1$ point to fit all of the data:

$$\tilde{P}_L = \frac{m_L 0.151}{m_L 0.151 + 0.849}. \tag{7}$$

The simulation and analytic solution agree for small M. Logically enough, as M grows, particles on the left can be replaced in a time smaller than $r/|v|$, at which point they can no longer penetrate the void at all (cf. Fig. 5, for time $<r/|v|$). This results in a drop-off of the simulation penetration rate.

We reproduced this experiment in (as nearly as possible) a lattice-free simulation as well. The geometry for this simulation is shown in the inset to Fig. 7. Here the dark gray particle is trapped between a wall to the left, which moves downward with mean speed V_s, and a second, static, wall to the right, containing a single void space. The positions of the particles on the two walls are randomized with the condition that a channel that is at least wide enough for the dark gray particle to traverse must remain. Once particles in the moving wall fall below a fixed height, they are removed from the simulation and replaced at a new, partially randomized location at the top of the wall. Similarly, once the dark gray particle falls below the same fixed height, it is removed from the simulation and replaced at a height of 3 particle spacings above the void, and a new randomized kick direction is applied. A competing particle is also provided, as shown in black; the magnitude of its kick, V_k, is the same as for the dark gray particle. In this way, as V_s/V_k is increased, the dark gray particle passes the void numerous times and so is provided with multiple opportunities to penetrate the void. Particle properties are as before, with the exception that the wall particles are taken to have a mass 10^9 times the mass of the competing particles. This prevents wall particles from

escaping laterally from the simulation. To prevent the dark gray particle from climbing out of the top of the simulation, it was necessary in addition to include a small gravitational acceleration for this particle alone.

In the main part of Fig. 7 we plot the results of this simulation. We again present an analytic result from Eq. (6); however, in this case, the gray particle can leave through the bottom, so even asymptotically at large M we cannot expect to achieve $P_L=1$. The simplest *a priori* estimate, given that the dark gray particle can leave the simulation through either of two possible exits, would be that $P_L=0.5$ asymptotically. In fact, the black particle competes for the void position, so P_L is less than this value. We evaluate P_L asymptotically by performing a simulation with large M ($M=100$), which gives $P_L\rightarrow 0.426$. Using this value and the $M=1$ simulation value as fit parameters, we find

$$\widetilde{P}_L = 0.426\,\frac{m_L 0.474}{m_L 0.474 + 0.526}, \tag{8}$$

which we plot as a solid line in Fig. 7.

The horizontal scales for the pseudolattice and continuum simulations are identical. For the continuum case the number of opportunities is taken to be $\langle V_s\rangle/V_k$, where $\langle V_s\rangle$ is the measured mean vertical velocity of the dark gray particle. Agreement seems reasonable between both the pseudolattice and continuum simulations and the analytic result predicted from Eq. (6).

We turn next to two example problems: flow along a boundary and bulk flow in a 2D tapped container. Our approach in both cases is to separate the convective flow into two distinct stages: a dilation stage, during which voids are introduced, and a subsequent relaxation stage, during which material settles to fill the voids. Dilation is experimentally observed to promptly follow a vertical tap to a resting mass of particles, and we assume that the dilation stage has the effect of nearly randomly introducing voids into the mass. It is during the relaxation stage that these voids are filled according to stochastic relations, such as Eq. (6). We remark that this construction, in which dilation and relaxation stages are distinguished, is a theoretical *necessity* for convective motion [10]. That is, the existence of convection relies on the fact that particles follow different trajectories on their way up and on their way down. If particles were to rise and fall according to the same, reversible, rule (or, equivalently, if particulate flow were to obey a single convective equation during each stage), then convection could not occur.

C. Example 1: Boundary flow in a 2D tapped container

Let us consider a simple example to start with. Following an upward impact to a square container partially filled with grains, it has been observed that particles within a fixed distance from the side walls of the container initially remain fixed with respect to the walls, while particles further into the container dilate in response to the impact [7]. This motivates us to study a column of particles (which we associate with particles near a wall) adjacent to another column containing a number of voids (simulating material in the bulk). This is a convenient first problem because it can be modeled as a one-dimensional stack of particles that leak out into the bulk in a prescribed way. In Fig. 8, we sketch a stack of particles at several successive times. We divide the stack vertically into equal segments of height Δz (expressed in units of particle diameters).

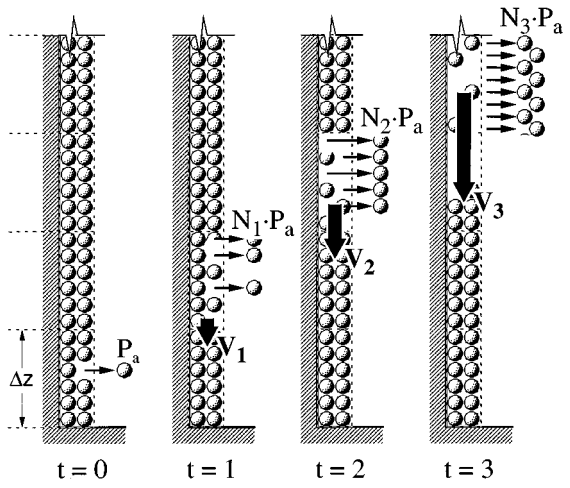

FIG. 8. Schematic of particle egress from boundary layer into bulk at successive times. At time $t=0$, a fraction P_a of particles in a unit height Δz escape from the boundary layer. A short time later, at time $t=1$, the particles supported by this unit height fall with speed V_1, resulting in an enhanced penetration probability, $N_1 P_a$. This process is amplified as time and height in the boundary layer increase.

We denote the probability that a particle leaves the lowest, stationary segment of the stack for the bulk P_a, and after an impact the stack can, on average, settle by moving

$$N_1 = P_a \rho_v \Delta z \tag{9}$$

particles downward, where ρ_v is the void fraction adjacent to the boundary layer.

The probability that a particle leaves the second segment from the bottom is then prescribed by Eq. (6), where m_L is the number of opportunities for penetration presented to each void. This number in turn is $m_L=1+N_1/w$, where w is the width of the boundary layer expressed in particle diameters. So the number of particles that can be expected to leave the second segment is given by

$$N_2 = \frac{m_L P_a}{m_L P_a + P_b + P_0}\,\rho_v \Delta z \tag{10}$$

$$= \frac{w + N_1}{(w/\beta) + w + N_1}\,\rho_v \Delta z, \tag{11}$$

where P_b and P_c are the numbers of voids adjacent to the second segment, which would be filled from directly above and from the bulk, respectively, and $\beta = P_a/(P_b+P_c)$. Notice that for the typical case, where material predominantly settles directly downward into voids, $P_a \ll P_b$, so $\beta \ll 1$. In this limit, we find

$$N_2 \approx (1 + N_1/w)\,\beta \rho_v \Delta z, \tag{12}$$

or, more generally, the number of particles leaving the kth segment for the bulk is

$$N_k \approx \left(1 + \frac{N_{k-1}}{w}\right) \beta \rho_v \Delta z. \tag{13}$$

This is equivalent to

$$N_k \approx (\beta \rho_v \Delta z/w) \frac{1-(\beta \rho_v \Delta z/w)^{k-1}}{1-(\beta \rho_v \Delta z/w)} w + (\beta \rho_v \Delta z/w)^{k-1} N_1. \tag{14}$$

Thus, in this approximation, the number of particles leaving the boundary layer increases exponentially to leading order with height from the bottom of the container. Since these particles support the particles above them, we can alternatively write that the downward velocity of particles (expressed as the number of particles moved per tap) grows with height according to

$$V_k = \sum_{j=1}^{k} N_j, \tag{15}$$

and, using the approximation that $\beta \rho_v \Delta z \ll 1$, we find

$$V_k \approx (\beta \rho_v \Delta z/w) N_1 + kw(\beta \rho_v \Delta z/w) - (\beta \rho_v \Delta z/w)^{k+1} N_1 \approx (\beta \rho_v \Delta z N_1/w) + (\beta \rho_v) z - (\beta \rho_v \Delta z/w)^{(z+\Delta z)/\Delta z} N_1, \tag{16}$$

where z is the number of particles (i.e., the height) from the bottom of the container. Equation (16) gives an explicit prediction for the dependence of vertical velocity on height in the boundary layer of a periodically tapped container of grains. We especially draw attention to the signs in this equation: the linear terms must be positive, while the exponential term must be negative. Consequently, we expect the boundary velocity to increase with height, possibly to a maximum value, and thereafter to diminish. We compare this prediction with two different types of numerical simulations in subsequent sections.

This result is based on several explicit and tacit assumptions. (1) The analysis assumes that particles settle starting from the bottom of a stack of particles and working upward to the top. This assumption is crucial, for it defines the mechanism by which velocities are amplified higher up in the stack. We remark, however, that the results should not be expected to hold for very tall containers of grains. In these problems, particles may settle within multiple, independent, vertically separated bands [18]. (2) The rate of transverse particle motion is assumed to be related to the relative vertical velocity of neighboring columns of particles. We have employed a particular stochastic description of this relation; other descriptions might work as well. (3) The distribution of voids is assumed to remain uniform with height. This permits us to use the simplification that the void fraction ρ_v is constant. This assumption is not crucial, but it simplifies analysis. (4) The analysis applies to experiments in which all of the grains in the container come completely to rest following each impact. (5) The probability of filling a void from above is assumed to greatly exceed that from the side. (6) The derivations are chiefly applicable far from the bottom of the container. Near the bottom, analysis is still possible in principle using Eq. (13), but it should be kept in mind that there will be no justification for expecting ρ_v to be independent of height there.

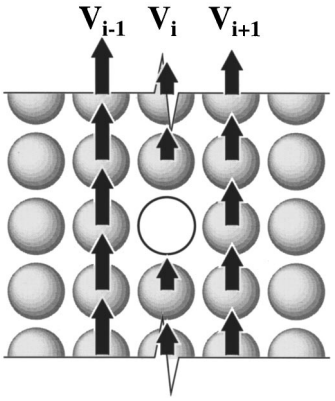

FIG. 9. Generic situation where a void can be penetrated from streams on either side, moving with different relative velocities. V_j represents the vertical velocity of the jth column of particles.

Finally, the boundary flow is driven in this scenario by the presence of voids in the bulk, and their absence along the boundary. This void contrast, coupled with the velocity dependence of void penetration [Eq. (6)], is what produces the complex flow, Eq. (16). Presumably, the experimentally observed void contrast is produced by friction and packing variations [19] between the particles and the container walls. This suggests that the downward boundary flow should be impeded in containers with polished walls and augmented in containers with roughened walls.

D. Example 2: Bulk flow in a 2D tapped container

We turn our attention next to the flow in the bulk of a tapped container of granular material. We begin with the observation that a simple shear cannot sustain net flow under isotropic conditions. This is due to symmetry: in a uniform shear field, the relative velocity between any two adjacent streams of particles is constant, and, using Eq. (16), a void stands an equal *a priori* chance of moving in either direction. Barring an externally provided anisotropy, we expect voids—and, consequently, material particles—to wander randomly and without bias. This situation changes in flows with differential shears. In these flows, we show that particles tend to migrate to regions of low shear in a way that can be modeled by a difference equation.

Earlier we considered the special case in which particles move only on one side of a void [Fig. 4(b)]. Now we study the more general problem in which particles on either side of a void can move (Fig. 9). Here we assign a relative vertical velocity (more precisely, a net displacement suffered by a column with respect to its neighbors during settling) $\Delta V_L = V_{i-1} - V_i$ on one side of the void and a different relative velocity $\Delta V_R = V_i - V_{i+1}$ on the other. As before, the effect of the relative velocities is to provide additional scattering opportunities that may enhance the probability for a particle from one side or the other to enter the void.

In Eq. (6), we wrote the probability for a void to be filled subject to a moving stream of particles on one side; we can write the corresponding formulas for streams of particles on both sides:

$$P_L=\frac{m_L P_1}{m_L P_1+P_2+m_R P_3},$$

$$P_R=\frac{m_R P_3}{m_L P_1+P_2+m_R P_3}, \tag{17}$$

where the numbers of opportunities to fill the void from the left or the right are, respectively, m_L and m_R. These numbers in turn depend on ΔV_L and ΔV_R according to

$$m_L=1+|\Delta V_L|,$$

$$m_R=1+|\Delta V_R|. \tag{18}$$

So if we again adopt the approximation that voids are predominantly filled from directly above, then $P_2 \gg m_L P_1 + m_R P_3$, and we find

$$P_L \approx (1+|\Delta V_L|)\beta_1,$$

$$P_R \approx (1+|\Delta V_R|)\beta_3, \tag{19}$$

where $\beta_1 \approx P_1/P_2$ and $\beta_3 \approx P_3/P_2$. Thus the flow into a void from either side is proportional to the relative velocities of constituent particles with respect to the void. The difference in probabilities for the motion of a void to either side is

$$P_L-P_R \approx (\beta_1-\beta_3)+(\beta_1|\Delta V_L|-\beta_3|\Delta V_R|). \tag{20}$$

For isotropic problems (e.g., far from boundaries), we can set $\beta_1=\beta_3$, and the number of particles that we expect to flow into the center column from either side is, therefore,

$$U_2=\rho_v(P_L-P_R)\approx \rho_v\beta_1(|\Delta V_L|-|\Delta V_R|). \tag{21}$$

Conservation of particles implies that, neglecting packing differences, as a particle moves from one column to an adjacent one, the column that receives the particle must increase in height by one particle diameter. Consequently, the vertical velocity of a column following a tap depends on the number of particles that are deposited into the column. That is, the increase in a column's vertical velocity is proportional to U_2. Thus we write

$$\zeta \frac{\Delta V}{\Delta z} \approx \xi^2 \rho_v \beta_1 \frac{\Delta^2 V}{\Delta x^2}, \tag{22}$$

where ζ and ξ are characteristic vertical and horizontal lengths for the problem. We use the suggestive notation $\Delta^2 V \equiv |V_1-V_2|-|V_2-V_3|$, and in order to algebraically separate physically distinct terms, we rewrite this equation as

$$P_2\zeta \frac{\Delta V}{\Delta z} \approx \rho_v P_1 \xi^2 \frac{\Delta^2 V}{\Delta x^2}, \tag{23}$$

where Δx is the separation between particle centers (roughly given by the particle diameter), and Δy is their vertical separation.

This is a difference equation that, subject to the approximations detailed above, governs granular flow in the bulk of a tapped container. Consider a few properties of this equation. First, solutions to Eq. (23) that are reflectionally symmetric about $x=0$ include

$$V=V_0+V_1\cosh(x/\sqrt{\rho_v P_1 \xi^2})e^{z/P_2\zeta}. \tag{24}$$

This result is in agreement with careful experimental work in which the precise flow field in tapped containers of grains has been measured directly [20].

Second, convective behavior as a function of z is not prescribed by Eq. (16) alone; it depends on the system size as well, since the response in the bulk is driven by inflow from the boundary. In smaller systems (i.e., where $w/\xi \sim 1$), the vertical flow can be expected to be dominated by boundary effects, and the z dependence in the bulk should obey Eq. (10). In larger systems (i.e., $w/\xi \ll 1$), on the other hand, Eq. (16) should hold in the bulk. By examining Eqs. (10) and (16), we find that the length scale over which material is driven into the bulk from the boundary is $L_b \equiv w/\rho_v$, while the length scale over which the bulk responds is $L_B \equiv P_2\zeta$. Thus, tall, narrow containers should have $L_b \ll L_B$ and boundary effects [Eq. (10)] should dominate, while short, broad containers should have $L_b \gg L_B$ and Eq. (16) should hold.

Third, the amplitude of convection can be expressed as a function of driving parameters by making use of Eq. (4). In that equation, we showed that the size of void space produced between an inelastic mass and a supporting platform that vibrates according to $z=A\sin(\omega t)$ obeys a simple relation for sufficiently high frequency. It stands to reason that the void fraction in the bulk ρ_v, will be simply proportional to this void size. Thus, we expect

$$\rho_v \cong C\left(10.54A-\frac{48.34g}{\omega^2}\right), \tag{25}$$

with some proportionality constant C. Although we are considering here sinusoidal vibration of the container, we assume that we are still operating in a regime where the grains come to rest between one cycle of vibration and the next [20]. Together with Eq. (24), this implies a particular form for the dependence of the convective velocity V on A and ω. That is, at any fixed location (x_0,y_0),

$$V(x_0,y_0)=C_0+C_1\cosh(C_2/\sqrt{A-C_3/\omega^2}), \tag{26}$$

where C_0, C_1, C_2, and C_3 are constants. For the special case where the acceleration $\gamma=A\omega^2$ is held fixed, this becomes

$$V(x_0,y_0)=C_0+C_1\cosh(C_4\omega), \tag{27}$$

where $C_4=C_2/\sqrt{\gamma-C_3}$. It is understood that the frequency in Eq. (27) is measured above an onset value; for frequencies below this value, the convective velocity vanishes. There is some experimental evidence [21] that indicates that for this case the velocity is exponential in ω. It would be interesting to determine whether Eq. (27) in fact fits the data.

Finally, a complete set of solutions to Eq. (23) includes reflectionally antisymmetric basis functions:

$$V=V_0+V_1\sinh(x/\sqrt{\rho_v P_i \xi^2})e^{z/P_2\zeta}. \tag{28}$$

In simple rectangular containers, we expect to see symmetric solutions of the form (24); in asymmetric containers, C^1 compositions of Eqs. (24) and (28) are possible. One addi-

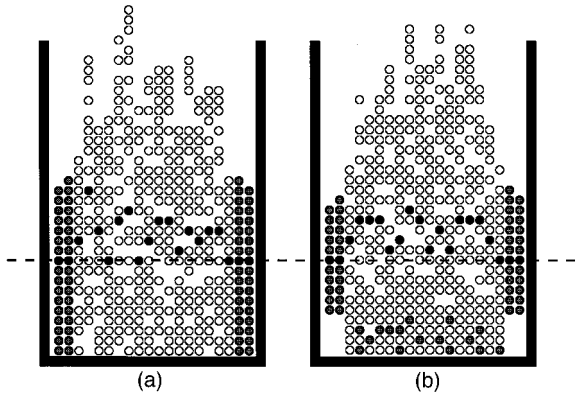

FIG. 10. Initial state of lattice immediately following a tap. (a) Voids randomly distributed in interior; (b) particles in corners moved to fill interior voids. Gray shaded particles along boundaries are held fixed initially. Black shaded particles are markers, initially placed in a horizontal line, ten particles from the bottom.

tional possibility may occur in containers with periodic boundary conditions [22]. In that case, it is possible to obtain solutions periodic in x, provided that the solutions *decay* with height; for example,

$$V = V_0 + V_1 \cos(x/\sqrt{\rho_v P_1 \xi^2}) e^{-z/P_2 \zeta}. \tag{29}$$

III. CELLULAR AUTOMATA SIMULATIONS

We can test these results in numerical simulations using the following algorithm [23]. For simplicity, we fix particles on a rectangular lattice. As we show, this approximation is sufficient to generate data largely in agreement both with preexisting experiments and with the preceding analysis. To complete the description of the problem, we need to specify initial and boundary conditions [24]. Throughout our simulations, we take the mean initial void fraction to be $\rho_v \cong \frac{1}{4}$. In Fig. 10, we show two possible initial configurations of voids. In Fig. 10(a), we show an initially random [10] set of voids in the bulk, with no voids along a narrow side boundary layer (shaded gray). We randomly assign void locations within the bulk (and displace supported particles upward as need be) because there are no good experimental [25] studies to guide us in the correct placement of voids immediately following an impact. We include no voids near the side boundaries in keeping with experimental reports that do exist [7]. In Fig. 10(b), we sketch a slightly different initial state, in which voids are inserted in boundary layers nearest the corners of the container; the particles coming from these voids are displaced horizontally to occupy the nearest previously allocated voids in the interior (displaced particles still shaded gray). The inclusion of this second initial state in our simulations is motivated by the following speculation [7]. Video footage [26] taken of vibrated containers filled with grains indicates that a large void initially forms at the bottom and center of a container during the vibration cycle. It appears from the video frames that the static boundary layers adjacent to the void then collapse into the void before the mass of grains above has the chance to fully relax back to the bottom of the container. It has been speculated that this collapse plays a major role in driving the ultimate convective motion of the grains [27]. To investigate this speculation, we include this scenario in our simulations. We have also studied the effects of eliminating the random allocation of voids in favor of placing voids only at the bottom and center of the container. The convective flow resulting from this initial state differs only slightly from the flow that we present, and, since the random allocation of voids [16] seems less *ad hoc* to us we choose the random case here.

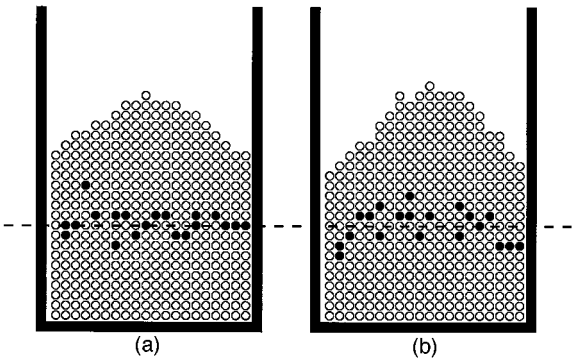

FIG. 11. Final state of lattice following upward percolation of all voids for the initial states shown in Fig. 10.

Given an initial configuration of voids, the next computational step is to percolate the voids upward. The rule for percolation is prescribed from our analysis: voids must move [28] directly upward with fixed probability P_2 and diagonally upward to the left or right with probabilities P_1 and P_3. We consider the symmetric case [29] $P_1 = P_3$. At every vertical height h starting from the bottom of the collection of particles, we perform the following computational tasks. First, we allow particles nearest the bottom to percolate downward one level. Next, we allow particles one level higher to percolate a level down, and so forth, up to the height h. We repeat this process until all particles below h come to rest (i.e., all voids reach the surface of the descending particles). At this point, we increment h by one particle diameter and repeat the process.

To observe the convective flow field, we track a line of marker particles. For example, in Fig. 10 we show (in black) the locations of marker particles initially placed ten particles

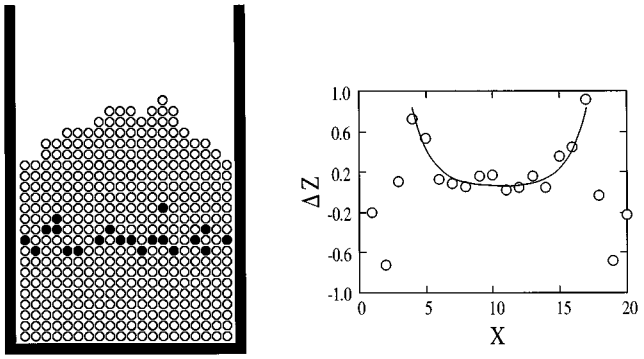

FIG. 12. 400 particles on lattice; each simulated tap delivers 96 voids at random into the interior of the heap. A two-particle-wide boundary layer along each side receives no voids initially. Left: shape of heap with initially horizontal marker particles (placed at a height of ten particle diameters) after 300 taps. Right: circles give average positions of marker particles over 300 successive taps; line gives fit to Eq. (24).

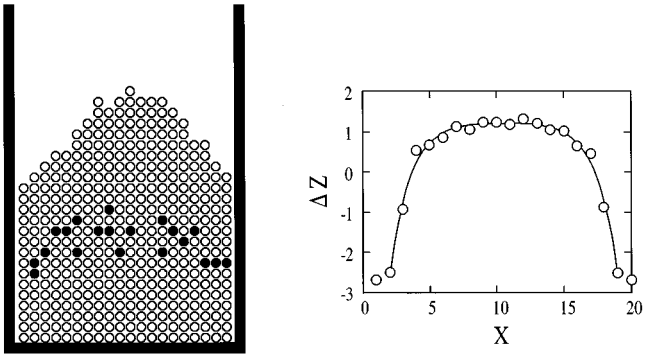

FIG. 13. 400 particles on lattice; each simulated tap delivers 96 voids at random into the interior of the heap. Eight voids are delivered into the bottom of each side of a two-particle-wide boundary layer and these 16 particles are distributed at random into the lowest existing voids in the interior. Left: shape of heap with initially horizontal marker particles (placed at a height of ten particle diameters) after 300 taps. Right: circles give average positions of marker particles over 300 successive taps; line gives fit to Eq. (24).

from the bottom (dashed line) immediately after the tap. In Fig. 11, we show the locations of the same particles for both cases of initial states after the voids have percolated upward. Notice that the qualitative behavior is similar for both initial states. For example, the final surface of the pile forms a rounded heap, and the marker particles have been scattered by the flow. Several quantitative differences exist, however, as we discuss next.

A. Zero corner voids

Let us first examine the naive initial state shown in Fig. 10(a). In this case, the cosh solution presents itself as a concave-up curve, as shown on the right of Fig. 12. In the figure, we apply 300 successive taps and display the averaged displacements of each of the marker particles on the right. On the left, we show the displacement incurred between the 299th and the 300th tap. The solid curve plotted on the right is a best fit to a cosh excluding the three points nearest the boundary [30] on either side and has correlation coefficient 0.95. The mechanism that leads to this curve seems to be as follows. Particles in the initially static boundary layer become entrained into interior voids. When this occurs, the boundary layer falls, demonstrated by the negative displacements near the walls shown on the right of Fig. 12. These particles are delivered primarily to the columns immediately adjacent to the boundary layer, so these columns increase their ultimate height by a corresponding amount. Finally, the cosh behavior predicted is seen in the interior of the lattice, subject to the boundary condition established by the columns adjacent to the boundary layer. The horizontal wave number predicted by Eq. (24) for the cosh solution is given by $k_x = 1/\sqrt{\rho_v P_1 \xi^2} \cong 0.63$. This agrees with the fit shown below, which has $k_x = 0.7 \pm 0.2$.

B. Added corner voids

If we include voids in the corners of the container, as shown in Fig. 10(b), the flow undergoes a distinct transformation. In Fig. 13, we repeat the simulations of Fig. 12 under precisely identical conditions except that eight new voids are added in each of the corners along the two-particle-wide boundary layers [31]. Now the concave-up cosh solutions switch to concave-down cosh solutions. The fit is again good, with correlation coefficient 0.99. The horizontal wave number predicted by Eq. (24) for the cosh solution here is again $k_x \cong 0.63$, which once more compares favorably with the fit to the simulation data with $k_x = 0.66 \pm 0.05$.

From these comparisons we conclude that the x dependence of the displacements resulting from discrete taps is well described by Eq. (24) from our model, irrespective of the details of the boundary conditions. The character of the flow that results depends sensitively on these details, however. In particular, these results support the speculation of Ref. [7]: the collapse of boundary particles from the lower corners of the container into the bulk flow does seem to drive the concave-down cosh flow observed in convection experiments [32].

C. Different aspect ratios

The same behavior holds for other aspect ratio lattices as well. In Figs. 14 and 15, we show results for lattices with aspect ratios 1:2 and 2:1 and approximately the same total number of particles and voids as in Figs. 12 and 13. In all cases, a two-particle-wide static boundary layer is used. Again, particles flow down the sides of the container, up the center, and good cosh fits are observed in the interior; correlation coefficients for the fits shown in Fig. 14 are 0.97 and

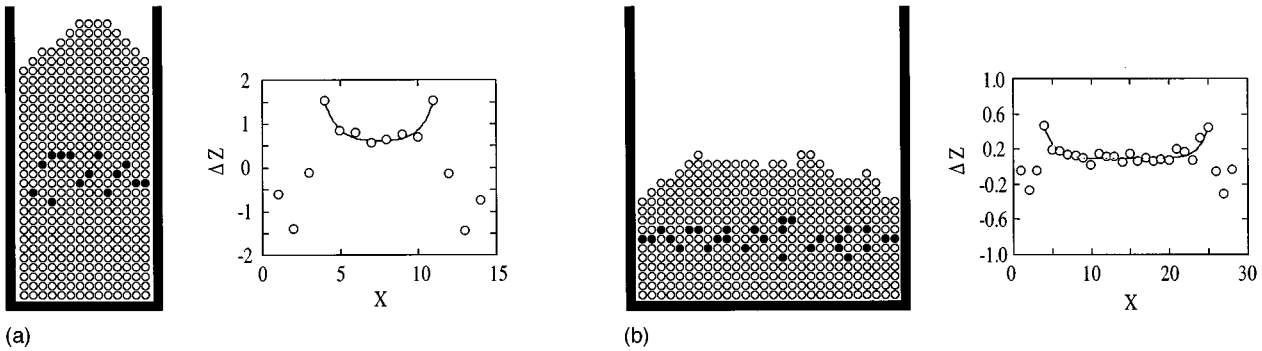

FIG. 14. Lattices containing (a) 28×14 and (b) 14×28 particles with initial conditions, as in Fig. 12. Marker positions are shown to left of graphs and circles in graphs give average positions of markers over 300 taps, while lines give fits to Eq. (24).

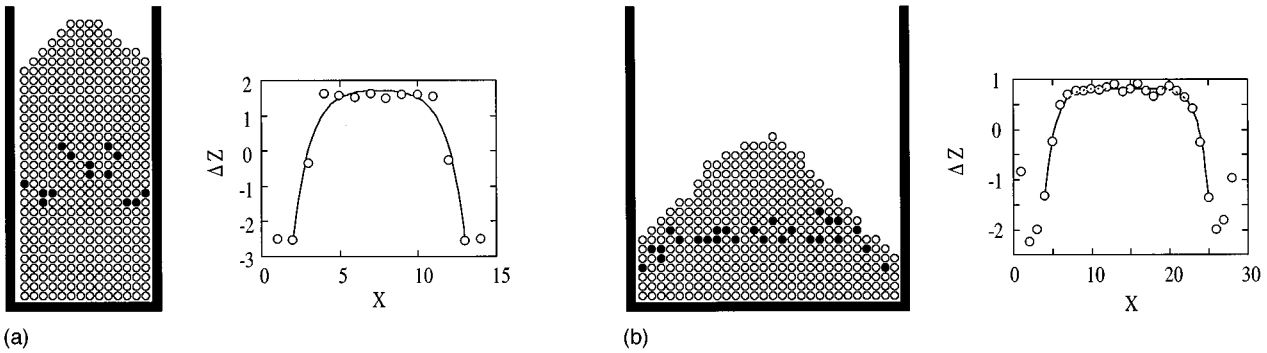

FIG. 15. Lattices containing (a) 28×14 and (b) 14×28 particles with initial conditions as in Fig. 13. Marker positions are shown to left of graphs and circles in graphs give average positions of markers over 300 taps, while lines give fits to Eq. (24).

0.92. With added voids in the corners (Fig. 15), the fits are also good, with correlation coefficient 0.99 for both aspect ratios shown.

D. Vertical dependence

We can also use this model to investigate the vertical dependence of the displacement following a tap. In Fig. 16 we show the displacement of an initially vertical line of marker particles (following 300 successive taps) placed in the horizontal center of the particle lattice both immediately following a tap and after the particles have settled. In the results that follow, we include excess voids in the corners of the container as discussed in the preceding section, since this initial state seems to best conform to experimental convection data. We apply 300 successive taps and display the averaged displacements of each of the marker particles in Fig. 17. In the figure we also include a fit to Eq. (16) using the lowest 14 marker particles [33]. The reason for fitting only the lowest 14 particles can be discerned by examination of Fig. 17: particles above this point are strongly influenced by the surface flow over the outside of the heap. This flow is well captured by the simulation, but is not a part of the analysis leading to the prediction of a linear-exponential dependence of displacement on height [Eq. (16)]. These results indicate possible avenues for experimental validation.

IV. PARTICLE-DYNAMICS SIMULATIONS

A. Velocity profiles

To validate our theoretical results further, we have performed soft-particle-dynamics simulations [34]. We placed 409 particles in a two-dimensional container approximately 20 mean particle diameters wide and shook the container through 50 separate cosinusoidal vertical oscillations. Following each complete cycle, all particles were allowed to come to rest. The container itself was lined with stationary particles so that the friction against the container walls was identical to the interparticle friction. Particle diameters are polydisperse, with mean 3 mm and variance 0.1 mm. The amplitude of oscillation of the base was 1 cm, and the frequency of oscillation was 5 Hz, resulting in an acceleration $\Gamma = A\omega^2 \cong 4g$.

Results of these simulations are shown in Figs. 18–20. In Figs. 18(a) and 18(b) we show how an initially horizontal line of particles chosen midway up the stack of particles is displaced following one oscillation cycle, and in Fig. 18(c) we show (open circles) the average vertical displacements of these particles over 50 cycles [35]. For comparison, we also show a fit to a cosh as a solid line. The parameters of friction, coefficient of restitution, and elasticity are essentially chosen arbitrarily, and as a result the surface shape and velocity profile parameters do not correspond precisely with preceding plots (e.g., Fig. 13). Nevertheless, the fit to a cosh is excellent, with correlation coefficient 0.997, and the velocity profile is unequivocally concave-down. This is in qualitative agreement both with our stochastic void-penetration model and with experiments [6]. Quantitatively, the wave number and other parameters defining the displacement profile depend on material properties and differ therefore from the lattice case.

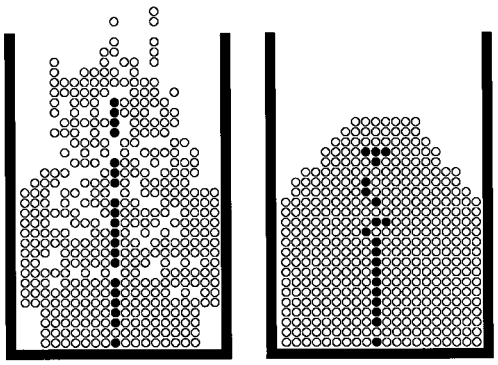

FIG. 16. Initial (left) and final (right) states of lattice with vertical array of marker particles.

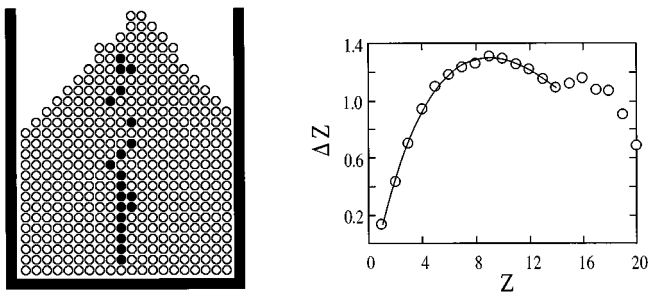

FIG. 17. Left: positions of initially vertical column of marker particles at center of lattice after 300 taps. Right: vertical displacements of markers versus initial height. Circles give averages over 300 taps; line is best fit to Eq. (16) of the 14 data points below the (shaded) surface.

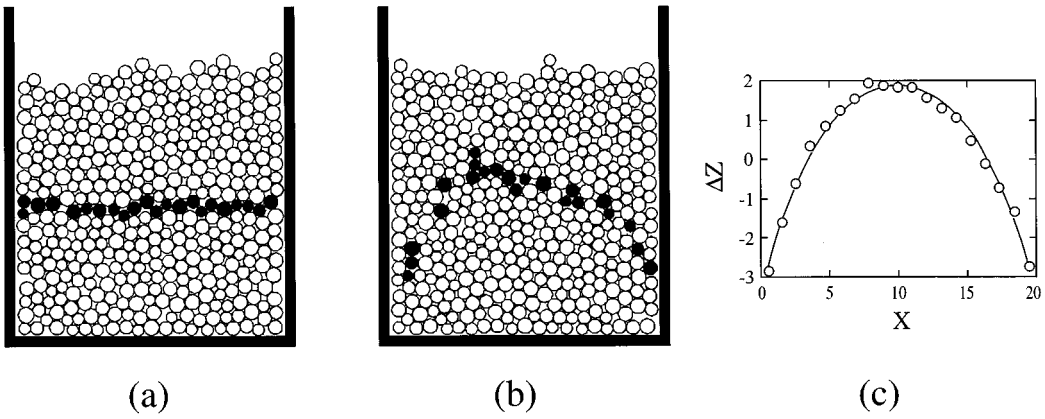

FIG. 18. Soft-particle-dynamics simulations of 409 particles shaken sinusoidally through 50 separate cycles. Polydisperse particles allowed to come to rest between cycles. (a) Particles before 50th cycle; marker particles (shaded black) chosen to have centers lying between 9.5 and 10.5 mean particle diameters from bottom. (b) Particles after 50th cycle; (c) mean vertical displacements of marker particles over 50 cycles (circles) and fit by cosh (line).

We have also evaluated the dependence of velocity profile on height within the stack of particles (cf. Fig. 17). These results, shown in Fig. 19, provide strong confirmation of the predictions of our model. As we mentioned earlier, the model requires that the vertical velocity increase, according to a particular linear-exponential law, where the linear term must have a positive coefficient and the exponential term must have a negative prefactor. In Fig. 19, we show the corresponding particle-dynamics simulation. In Fig. 19(c), we show, as open circles, the average over 50 cycles of vertical displacements of marker particles as a function of height [36]. We also plot, as a solid line, the fit to Eq. (16) with coefficients with the prescribed signs. The fit has correlation coefficient 0.991. As in Fig. 17, we exclude points near the surface (shaded gray).

B. Modified boundary flow

A final prediction from our cellular automata simulations is that the convective velocity field depends strongly on boundary conditions. For example, the convective velocity field studied here is evidently driven by a downward flow along the side walls. By interrupting this boundary flow, we should be able to transform the velocity field from a concave-down cosh [with a convex top surface defined by a distinct angle of repose—cf. Figs. 13, 14(a), and 15] to a concave-up cosh [with a flattened, possibly even concave, surface—cf. Fig. 14(b)]. Since the downward boundary flow can in turn only be driven by the downward flow of the side walls during shaking, one way to do this would be to move the bottom of the container down within a container with fixed walls. Alternatively, stepped or terraced side walls could be used to interrupt the boundary flow and generate a concave-up flow profile.

We have tested this prediction as well, using particle-dynamics techniques. In Fig. 20, we periodically lower only the bottom surface of the container, keeping the side walls fixed [37]. This interferes with the presumed downthrust of the boundary layer due to wall motion. In this case, we see a concave-up, small-amplitude (cf. Fig. 12) displacement profile.

CONCLUSIONS

By focusing on the dynamics of void motion, we have developed a model that duplicates many experimentally ob-

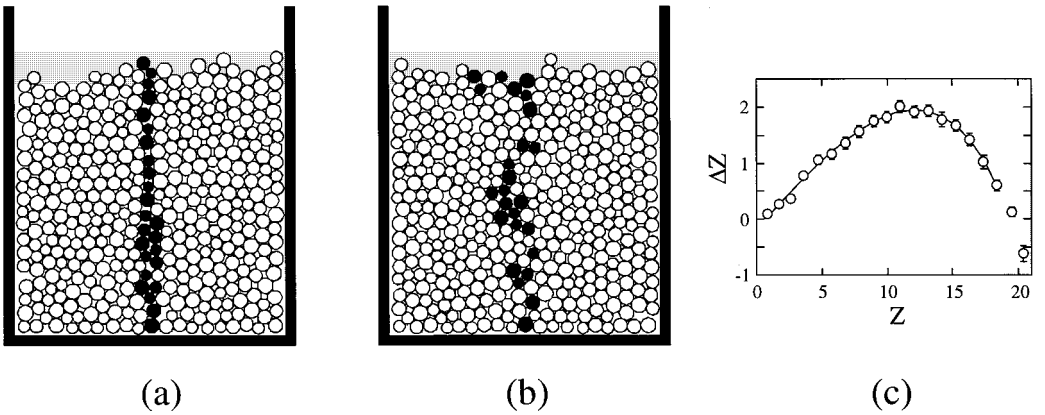

FIG. 19. Soft-particle-dynamics simulations as in Fig. 18, with marker particles (black) chosen to have centers between 9.5 and 10.5 particles from left wall. (a) Particles before 50th cycle; (b) particles after 50th cycle; (c) mean vertical displacements of marker particles over 50 cycles (circles) and fit to Eq. (16) (line). Particles very near the surface (shaded gray) are excluded from the fit.

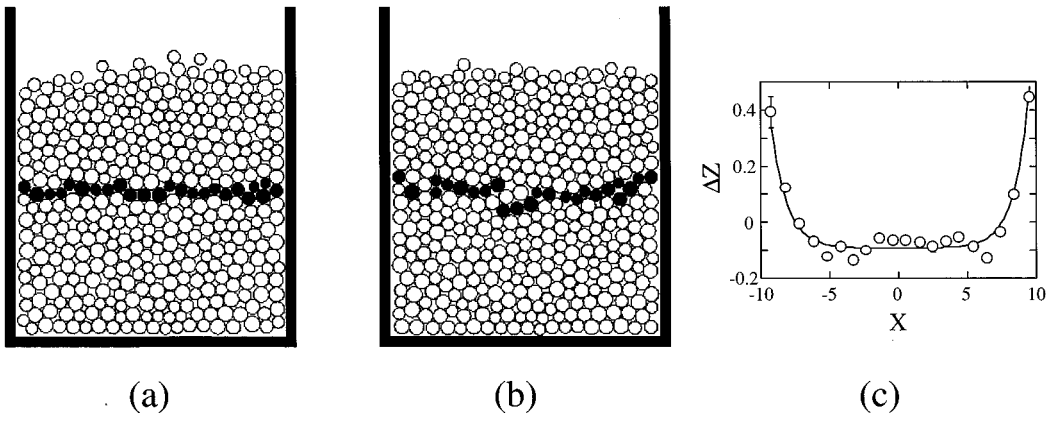

FIG. 20. Soft-particle-dynamics simulations of 409 particles, in which the bottom of container is periodically lowered but side walls are fixed through 50 separate cycles. Polydisperse particles allowed to come to rest between cycles. (a) Particles before 50th cycle; marker particles (shaded black) chosen to have centers lying between 9.5 and 10.5 mean particle diameters from bottom. (b) Particles after 50th cycle; (c) mean vertical displacements of marker particles over 50 cycles (circles) and fit to cosh (line).

served features of granular convection. Our results indicate that the qualitative mechanism driving granular convection may simply be that void penetration depends on relative velocities of adjacent particles. The role of this velocity differential is to provide additional scattering opportunities that may permit a particle from one side or the other to enter the void. Using this model, it is not difficult to understand the mechanism that drives particles toward regions of low shear: voids in a differential shear field are more likely to exchange places with particles in the direction with higher relative velocity. Conversely, particles will tend to migrate toward regions of low shear. This migration seems to be what leads to intriguing observed flow behaviors in granular convection.

Quantitatively, we conclude that the detailed behavior of the displacements resulting from discrete taps is well described by Eqs. (16) and (24) from our model. The character of the flow that results seems to depend rather sensitively on the specifics of the boundary conditions [38]. In particular, results suggest changes in convective devices that should significantly change the convective velocity field. For example, the convective velocity field studied here is evidently driven by a downward flow along the side boundaries. By interrupting this boundary flow, it should be possible to transform the velocity field from a concave-down cosh to a concave-up cosh. Since the downward boundary flow can in turn only be driven by the downward flow of the side walls during shaking, one way to do this would be to move the bottom of the container within a container with fixed walls. Alternatively, stepped or terraced side walls could be used to interrupt the boundary flow and generate a concave-up flow profile. This and other predictions remain to be experimentally tested.

ACKNOWLEDGMENTS

This work was gratefully supported by the Petroleum Research Fund and by the National Science Foundation, Division of Chemical and Transport Systems. T.S. wishes to thank R. Almgren, H. Jaeger, L. Kadanoff, J. Knight, and S. Nagel for their hospitality and many informative discussions.

[1] H. M. Jaeger and S. R. Nagel, Science **255**, 1523 (1992); R. P. Behringer, Nonlinear Sci. Today **3**, 1 (1993).

[2] F. Melo, P. Umbanhowar, and H. L. Swinney, Phys. Rev. Lett. **72**, 172 (1994); and unpublished; Y. Du, H. Li, and L. P. Kadanoff, Phys. Rev. Lett. **74**, 1268 (1995); H. K. Pak and R. P. Behringer, *ibid*. **71**, 1832 (1993); R. P. Behringer and G. W. Baxter, in *Granular Matter*, edited by A. Mehta (Springer-Verlag, New York, 1994), pp. 85–119.

[3] J. B. Knight, C. G. Fandrich, C. N. Lau, H. M. Jaeger, and S. R. Nagel, Phys. Rev. B **51**, 3957 (1995); F. Melo, P. Umbanhowar, and H. L. Swinney, Phys. Rev. Lett. **72**, 172 (1994).

[4] O. Reynolds, Philos. Mag. **20**, 469 (1885); *Papers on Mechanical and Physical Subjects* (Cambridge University Press, New York, 1901), Vol. II, p. 217; J. Duran, T. Mazozi, E. Clement, and J. Rajchenbach, Phys. Rev. E **50**, 3092 (1994); H. K. Pak and P. R. Behringer, Nature **371**, 231 (1994).

[5] An important exception is H. Caram and D. C. Hong, Phys. Rev. Lett. **67**, 828 (1991).

[6] J. B. Knight, E. E. Ehrichs, V. Y. Kuperman, J. K. Flint, H. M. Jaeger, and S. R. Nagel, Phys. Rev. E **54**, 5726 (1996); J. B. Knight, H. M. Jaeger, and S. R. Nagel, Phys. Rev. Lett. **70**, 3728 (1993).

[7] M. Bourzutschky and J. Miller, Phys. Rev. Lett. **74**, 2216 (1995).

[8] See, e.g., S. Luding, E. Clément, A. Blumen, J. Rajchenbach, and J. Duran, Phys. Rev. E **49**, 1634 (1994).

[9] S. McNamara and W. R. Young, Phys. Fluids A **4**, 496 (1992); S. McNamara and W. R. Young, Phys. Rev. E **50**, R28 (1994); Y. Du, H. Li, and L. P. Kadanoff, Phys. Rev. Lett. **74**, 1268 (1995); P. Constantin, E. Grossman, and M. Mungan (unpublished).

[10] A. Mehta, in *Granular Matter*, edited by A. Mehta (Springer-

Verlag, New York, 1994), p. 1.
[11] J. S. Walker and T. Soule (unpublished); W. Chin, E. Ott, H. E. Nusse, and C. Grebogi, Phys. Rev. E **50**, 4427 (1994); S. H. Shaw and P. Holmes, Phys. Rev. Lett. **51**, 623 (1983).
[12] E. Andersson (unpublished); H. K. Pak and R. P. Behringer, Phys. Rev. Lett. **71**, 1832 (1993); S. Douady, S. Fauve, and C. Laroche, Europhys. Lett. **8**, 621 (1989); Y.-H. Taguchi, Phys. Rev. Lett. **69**, 1367 (1992); E. E. Ehrichs, H. M. Jaeger, G. S. Karczmar, J. B. Knight, V. Y. Kuperman, and S. R. Nagel, Science **267**, 1632 (1995); M. L. Hunt, S. S. Hsiau, and K. T. Hong (unpublished).
[13] cf. E. Andersson (unpublished).
[14] The same arguments apply to other geometries. In an actual rectangular lattice, dilation would be required to permit void penetration from all sides; this effect is neglected in our simulations and, consequently, simulations performed on a hexagonal lattice produced essentially indistinguishable results.
[15] Ya. G. Sinai, Russ. Math. Surv. **25**, 137 (1970); S. Bleher, C. Grebogi, and E. Ott, Physica D **46**, 87 (1990); Q. Chen and M. Ding, Phys. Lett. A **115**, 93 (1990); M. Ding, C. Grebogi, E. Ott, and J. A. Yorke, Phys. Rev. A **42**, 7025 (1990).
[16] Our analysis does not rely on this restriction; it is included only to slightly simplify the algebra leading to the ultimate solution.
[17] See, e.g., G. C. Barker, in *Granular Matter* (Ref. [10]), pp. 35–84.
[18] cf. K. Ichiki (unpublished).
[19] Originally discussed in O. Reynolds, *Papers on Mechanical and Physical Subjects* (Ref. [4]).
[20] This is the situation in crucial experimental work: J. B. Knight, E. E. Ehrichs, V. Y. Kuperman, J. K. Flint, H. M. Jaeger, and S. R. Nagel, Phys. Rev. E **54**, 5926 (1996); E. E. Ehrichs, H. M. Jaeger, G. S. Karczmar, J. B. Knight, V. Y. Kuperman, and S. R. Nagel, Science **267**, 1632 (1995).
[21] J. B. Knight, E. E. Ehrichs, V. Y. Kuperman, J. K. Flint, H. M. Jaeger, and S. R. Nagel, Phys. Rev. E **54**, 5726 (1996); J. B. Knight, H. M. Jaeger, and S. R. Nagel, Phys. Rev. Lett. **70**, 3728 (1993).
[22] H. K. Pak and R. P. Behringer, Phys. Rev. Lett. **71**, 1832 (1993).
[23] Prior work using cellular automata to model granular flow includes: G. W. Baxter and R. P. Behringer, Physica D **51**, 465 (1991).
[24] We remark that the cellular automata simulations used to validate the analytic results can only encode particle positions and cannot encode particle velocities. This is clearly only an approximation. It should be borne in mind, for example, that the void distributions investigated are at best effective quantities which may not actually be seen at any instant in time.
[25] Particle dynamic evaluations of void distributions have been carried out [T. Shinbrot, D. V. Khakhar, J. J. McCarthy, and J. M. Ottino (unpublished)] and produce similar results to the initial state shown in Fig. 10(b).
[26] Videos produced by J. Knight, H. Jaeger, and S. Nagel.
[27] The effects of trapped gases on this motion can be significant [cf. H. K. Pak and R. P. Behringer, Nature **371**, 231 (1994)], but are neglected in this work.
[28] Naturally, these probabilities apply provided that there is a particle in the appropriate position that can fall to fill the void. If no particle is present, the given motion is disallowed and the void must be filled from elsewhere.
[29] To accomodate the earlier approximation that $P_2 \gg P_1$, we take $P_1 = P_3 = 0.1$ and $P_2 = 0.8$.
[30] As earlier remarked, our analysis applies only to the isotropic problem, far from boundaries where strong gradients in void content are expected.
[31] These eight particles from each side are translated horizontally to fill the nearest existing voids prior to void percolation.
[32] J. B. Knight, E. E. Ehrichs, V. Y. Kuperman, J. K. Flint, H. M. Jaeger, and S. R. Nagel, Phys. Rev. E **54**, 5726 (1996); E. E. Ehrichs, H. M. Jaeger, G. S. Karczmar, J. B. Knight, V. Y. Kuperman, and S. R. Nagel, Science **267**, 1632 (1995).
[33] We use the fit to Eq. (16) because it is a precise description of the number of particles input to the bulk from the boundary as a function of height. By continuity, we expect the integrated volume increase in the bulk to increase proportionately. Equation (24) could alternatively have been used, however, it gives the bulk response to (unknown) particle flux values and can be expected to be less accurate.
[34] P. A. Cundall and O. D. L. Strack, Geotechnique **29**, 47 (1979); J. J. McCarthy, T. Shinbrot, G. Metcalfe, E. Wolf, and J. M. Ottino, AlChE J. (to be published).
[35] These data are collected into 20 bins, evenly distributed in the range $-10 < X < 10$, in units of the mean particle diameter. Data within each bin are then averaged. Error bars are smaller than the plot symbol.
[36] These data are collected into 20 bins, evenly distributed in the range $0 < Z < 20$, in units of the mean particle diameter. Data within each bin are then averaged. Error bars are smaller than the plot symbol.
[37] This motion is similar to experimental work performed to study granular chute flow: O. Pouliquen and R. Gutfraind, Phys. Rev. E **53**, 552 (1996). In these experiments, concave-up flow profiles have been seen.
[38] E. E. Ehrichs, H. M. Jaeger, G. S. Karczmar, J. B. Knight, V. Y. Kuperman, and S. R. Nagel, Science **267**, 1632 (1995); M. Bourzutschky, and J. Miller, Phys. Rev. Lett. **74**, 2216 (1995); J. B. Knight, E. F. Ehrichs, V. Y. Kuperman, J. K. Flint, H. M. Jaeger, and S. R. Nagel, Phys. Rev. Lett. **54**, 5726 (1996).